Available online at www.sciencedirect.com

ScienceDirect

Procedia CIRP 111 (2022) 335–339

www.elsevier.com/locate/procedia

12th CIRP Conference on Photonic Technologies [LANE 2022], 4-8 September 2022, Fürth, Germany

Preliminary study to investigate the applicability of optical strain measurement technique for the detection of hot cracks in laser metal deposited layers

Anne Straße[a,*], Nasim Bakir[a], Andrey Gumenyuk[a,b], Michael Rethmeier[c,a,b]

[a]*Bundesanstalt für Materialforschung und -prüfung (BAM), Unter den Eichen 87, 12205 Berlin, Germany*
[b]*Fraunhofer-Institute Produktionsanlagen und Konstruktionstechnik (IPK), Pascalstraße 8-9, 10587 Berlin, Germany*
[c]*Technische Universität Berlin, Pascalstraße 8-9, 10587 Berlin, Germany*

* Corresponding author. Tel.: +49 30 8104 4864; E-mail address: anne.strasse@bam.de

Abstract

Laser metal deposition (LMD) as an additive manufacturing technique became increasingly important in recent years and thus the demand for component safety. This is the reason, for the need for reliable in-situ defect detection techniques. For laser beam weld seams an optical measurement technique based on an optical flow algorithm was successfully used to define the critical straining conditions that lead to hot cracking. This algorithm was adapted for bead-on-plate weld seams on LMD deposited layers of IN718 alloy while performing external strain on the specimen in an externally loaded hot cacking test facility. The resulting transversal hot cracks along the weld seam were localized via X-Ray inspection and the type of cracking confirmed by Scanning Electron Microscopy (SEM). The strain distribution was measured in the vicinity of the solidification front and correlated to the detected hot cracks. Based on the results this technique could be adopted for LMD experiments.

Keywords: Strain measurement; Optical flow; Critical strain; Laser Metal Deposition (LMD), Direct Energy Deposition of Metals by Laser Beam (DED/LB/M)

1. Introduction

In recent years laser metal deposition (LMD) or rather direct energy deposition of metals by laser beam (DED/LB/M) as an additive manufacturing (AM) technique became increasingly important and with it the demand for an advanced process monitoring/control and component safety. Especially in high temperature applications for safety critical components defects like hot cracking can have disastrous consequences.

Nickel-based superalloys, because of their good resistance against creep and an excellent tensile and fatigue strength at high temperatures, are often used for such high temperature applications [1, 2]. A known problem with those superalloys is their susceptibility to hot cracking in form of liquation cracks during cyclic thermal heating necessary for the layer wise building of the LMD process. One reason for the hot cracking is the so-called constitutional liquation, the existence of liquid material at temperatures below the solidus temperature [3].

Nomenclature

AM	Additive manufacturing
BTR	Brittle temperature range
CTW	Controlled tensile weldability
DED/LB/M	Direct energy deposition of metals by LB
f	Defocussing in mm
f_{CMOS}	Framerate CMOS-camera in fps
HAZ	Heat affected zone
LB	Laser beam
LMD	Laser metal deposition
P_S	Laser power in kW
ROI	Region of interest
v_s	Welding speed in m·min^{-1}

2212-8271
10.1016/j.procir.2022.08.034

Due to the high heating rate typical for laser beam welding, the phases in the heat affected zone (HAZ) are not completely dissolved resulting in grains surrounded by liquid films. When straining, typical during cooling, occurs those liquid films at the grain boundaries rupture. Due to the not liquified grains surrounding those cracks no molten material is provided, to fill those cavities. Typically, those liquation cracks are in the HAZ of the weld seam [4]. For the LMD process this means the prior layer. But this is not the only reasons for hot cracking, as it is always an interaction between the welding parameters, the metallurgy, and the straining conditions [5]. Pellini [6] reported hot cracking being a strain-controlled phenomenon, that occurs when the liquid films between the dendrites cannot withstand the accumulated straining, evoked by temperature gradients, exceeding a critical value. Whereas Prokhorov [7, 8] defines in his strain-based thermo-mechanical model a brittle temperature range (BTR), in which hot cracking occurs, when a critical strain is surpassed. The BTR is defined by solidus (T_S) and liquidus (T_L) temperature as well as the critical strain and the critical strain rate. Fig. 1 shows the BTR according to Prokhorov schematically [8, 9].

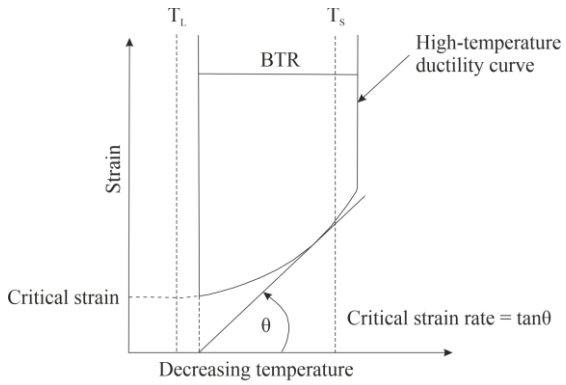

Fig. 1. Schematic illustration of the BTR during solidification [8, 9]

The determination of the actual straining conditions was and is object of many studies. But since LMD as well as laser beam (LB) welding are high temperature processes the process observation is challenging, due to e.g., laser reflections, emissions of secondary irradiation (hot metal, vapor and plasma) and spattering. One method is the measurement by means of In-Situ Observation (MISO)-technique developed by Matsuda et al. [10-12] With the help of a high-speed camera the formation of hot cracks is recorded, but due to smoke and smearing an exact observation is difficult. Bakir et al. [13] approached the weld pool up to a distance of 2 mm with digital image correlation (DIC), where a random splatter pattern is applied on the surface of the specimen, which can be detected in a deformed condition. In later studies the authors used the optical flow technique based on the Lucas-Kanade algorithm [14, 15]. To determine the critical straining necessary for hot cracking specimens are fixed in a controlled tensile weldability (CTW) test-facility and strained during bead-on plate partial or full penetration welding. With this setup Bakir et al. were able to detect critical strain as well as strain rate leading to solidification cracks in austenitic stainless steel 316L [15]. The same setup should be used for this study to investigate the straining conditions leading to liquation cracks in LMD coatings.

2. Experimental setup

The base material for the CTW-test specimen was an AISI S304L austenitic stainless steel with the dimensions of 80 mm x 460 mm x 4 mm. The specimens have a reduced section in the middle following the form of flat tensile test specimen. This reduced section had a width of 50 mm and a length between the shoulders of 60 mm. The length of the grip section was 200 mm. The specimen is visible in Fig. 2. As coating material an Inconel 718 (IN718) nickel-based superalloy powder was used. It had a particle size of 45 µm - 90 µm. This material combination was chosen, because of the good distinguishability of both phases in microsections and the hot cracking susceptibility of the additive manufactured coating.

Table 1. Chemical composition (wt.-%) of the materials

Elements	AISI304L (wt.-%)	IN718 (wt.-%)
Al	-	0.46
C	0.03	0.05
Co	-	0.06
Si	1.00	0.04
Mn	2.00	0.07
P	0.045	0.011
S	0.03	0.002
Cr	18.00 - 20.00	19.04
Mo	-	3.08
Ni	10.00 - 12.00	Bal.
Nb	-	5.16
Ti	-	0.80
Fe	Bal.	19.02

For both materials the chemical composition according to the manufacturer's specifications for the IN718 and DIN EN10088-3 [16] for the austenitic stainless steel is shown in Table 1.

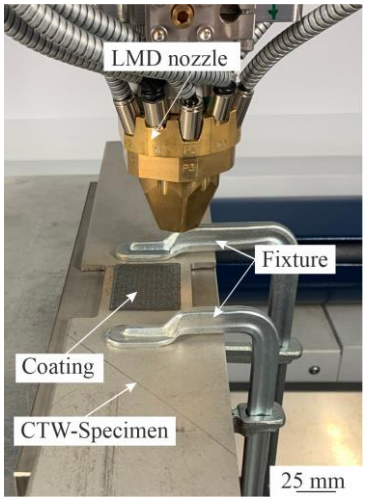

Fig. 2. Experimental setup for the coating by LMD

For the DED/LB/M/IN718 coatings a five-axis Trumpf TruLaser Cell 3000 working station, equipped with a 16 kW Trumpf TruDisc 16002 Yb:YAG-disc laser with the wave length of 1030 nm was used. The powder was deposited with a Medicoat Flowmotion Twin powder feeder. The powder feeding rate was 15 g·min^{-1}. The experimental setup is shown in Fig. 2.

The working distance of the coaxial six-jet nozzle was 25 mm with a powder spot diameter of approx. 2.8 mm. The coating parameters were a laser spot diameter of 2.8 mm, a welding velocity of 4.0 m·min^{-1} and a laser power of 2.0 kW. The coated area of 50 mm x 35 mm consisted of two layers with 26 overlapping tracks with a track width of approx. 2.8 mm and a stepover of 1.4 mm.

Fig. 3 shows the experimental setup for the CTW-Test of the coated specimen. It was conducted in a CTW-test facility equipped with the same Trumpf TruDisc 16002 Yb:YAG-disc laser used for the LMD coating. The testing machine clamps the specimen hydraulically with one moving and one unmoving clamp and allows for a maximum tensile load of 200 kN.

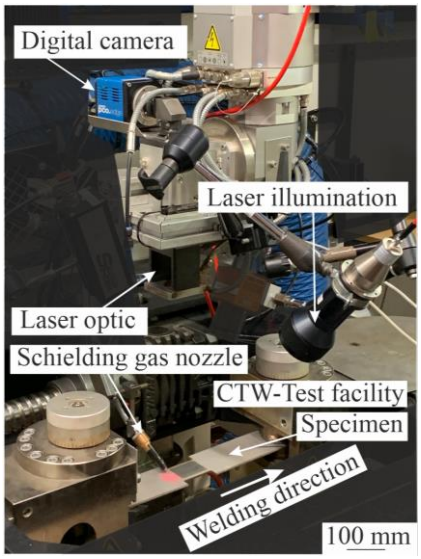

Fig. 3. Experimental setup for CTW-testing of LMD coated specimen

The process was recorded by means of a S-CMOS-camera installed parallel to the optical axis of the laser optical head. The camera has a maximum resolution of 2560 pixel x 2160 pixels with a maximum framerate of 200 frames per second. The specimen´s surface was illuminated with a Dilas diode laser with a maximum laser power of 100 W and a wavelength of 808 nm. The illumination laser as well as the CMOS-camera were moved along with the laser head. shielding gas for the coating as well as the CTW-test was argon.

Table 2. Experimental parameters

Parameter	value
Welding speed v_s in m·min^{-1}:	0.8
Laser power P_s in kW:	1.0
Defocussing f in mm:	57
Framerate f_{CMOS} in fps:	400
Resolution in pixel	460 x 240

The weld seam had a length of 60 mm and the specimen was elongated by 12 mm with a velocity of 160 mm·min^{-1} which corresponds to a global strain of 20 %, which was chosen to ensure hot cracking.

The used parameters are listed in Table 2.

3. Results and discussion

The outer appearance of the deposition layer on the plates does not perform any obvious oxidation and looks homogenous. For a better orientation the surface was marked with laser weld spots in a distance of 3 mm to each other, previous to the CTW-test. Those marks are shown in Fig. 4 (a) below the weld seam.

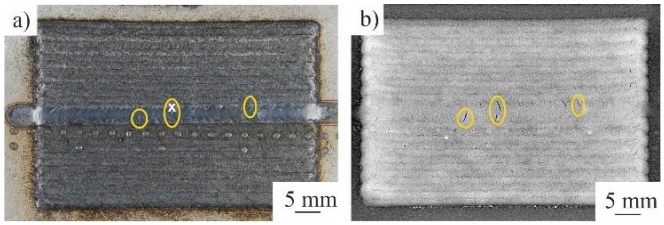

Fig. 4. (a) Photograph of LMD-coating after being subjected to CTW-test; (b) X-Ray image of the LMD-coated specimen after CTW-test (SEM-position marked with a cross)

The optical as well as the X-ray analysis (Fig. 4 (b)) of the coated area showed multiple cracks along the weld seam. The SEM (Fig. 5) analysis confirmed them to be liquation cracks. They arise in the HAZ and migrate into the weld seam due to the external strain being applied to the specimen.

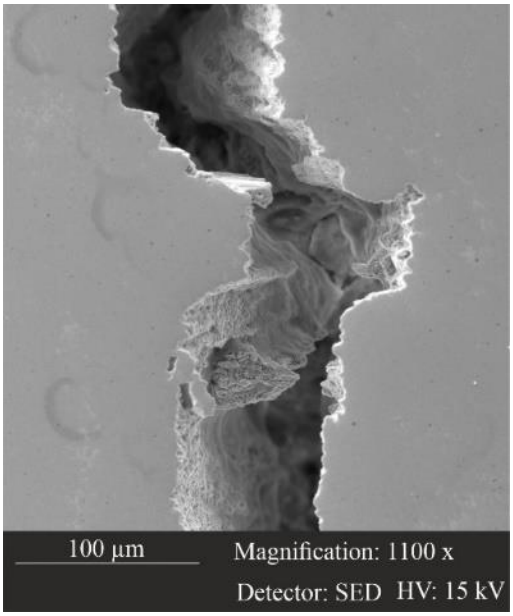

Fig. 5. SEM-picture of hot crack

The SEM image shows the liquation crack with the typical appearance of a smooth surface with dendrites tips revealed.

The analysis of the recorded video sequence of the CMOS-camera showed difficult optical conditions. Although several cracks were visible on the specimens surface their development was not directly detectable in the video.

The region of interest (ROI) was chosen directly behind the weld pool and analyzed by means of mean strain in welding direction. Its size was chosen 125 Pixels x 170 Pixels. Here the laser weld spots were used for orientation.

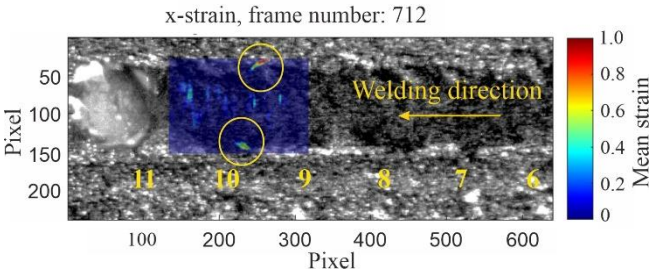

Fig. 6. Strain distribution in ROI for Frame 712.

The highest strains were visible at the margins of the weld line (marked positions in Fig. 6) immigrating into the weld seam, as is typical for liquation cracks and described in [3]. The analysis shows an increased mean strain in the areas of detected cracks, but since a lot of small cracks are visible in the X-ray image in Fig. 7 the strains are not always easily associated with a certain crack.

Fig. 7 also depicts the diagram correlating the mean strain to the X-ray analysis. It is visible that the graph shows irregularities. Those hint to the formation of hot cracks, since the global straining was applied before the start of the CTW-test. Consequently, the mean strain should remain stable without major irregularities. For the hot cracks between marker point 10 and 11 and 15 and 16 the peaks in the graph show the typical form of a steep ascent of the mean strain until reaching a critical value resulting in the crack opening and falling afterwards, as shown by Bakir et al. [15]. In case of the hot crack between marker point eight and nine, this peak is not visible.

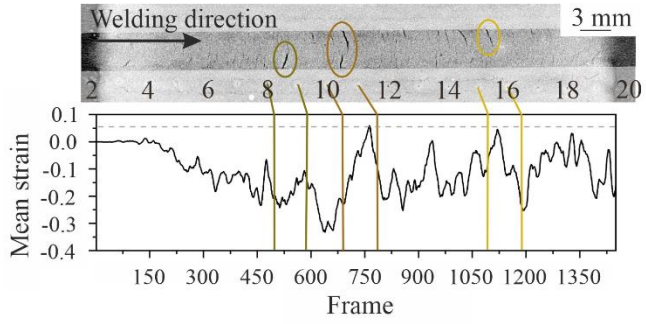

Fig. 7. Correlation of mean strain to X-Ray image.

Those results might be explained for one by liquation cracks being far smaller than solidifications cracks and thus harder to detect. The X-Ray analysis shows multiple hot cacks, some of them even visible on the surface of the specimen, but it is probable that those started as small cracks, represented by the increased strain in the ROI of the recorded video sequence and were opened by the high global strain rate. For a direct detection of the crack opening on the one hand, the resolution of the camera might not be high enough or on the other hand, the range of the video section might not cover enough of the weld seam behind the weld pool. Since a higher resolution with a wider field of view at the same time prelude each other, further experiments towards the determination of the exact moment of crack initiation must be conducted.

A second explanation for the results might be the location of the ROI for the mean strain analysis. Since liquation cracks start at the margin of the weld line the mean strain of the chosen ROI includes lots of noise, not necessary for the determination of the critical strain. For further analysis a relocation of the ROI as well as the used for the analysis must be improved.

4. Conclusions

A novel approach towards hot cracking detection for the LMD process was investigated. This approach was already successfully applied on laser beam weld seams for the detection of solidification cracks. In this preliminary study the aim was the detection of liquation cracks. For this LMD coated flat specimen were produced and subjected to bead-on laser beam welds in a CTW-test facility under 20 % global strain.

The welding process was observed with a CMOS camera and subsequently the straining conditions analyzed by means of optical flow algorithm. The results of this preliminary study show, that the exact moment of crack initiation was not yet recorded, but that a general detection of the mean strains was possible. The existing analyzing technique needs further improvement but has considerable potential.

Acknowledgements

The authors would like to thank Department 8.3-Radiological Methods, namely Mr. Marcel Grunwald for providing the X-Ray images.

References

[1] Kumar, S., Rao, G.S., Chattopadhyay, K., Mahobia, G., Srinivas, N., and Singh, V.: Effect of surface nanostructure on tensile behavior of superalloy IN718, Materials & Design, 2014; 62, pp. 76–82.
[2] Sharma, A.D., Sharma, A.K., and Thakur, N.: Crystallographic, microstructure and mechanical characteristics of dynamically processed IN718 superalloy, Journal of Alloys and Compounds, 2014; 597, pp. 175–180.
[3] Radhakrishnan, B., and Thompson, R.G.: A phase diagram approach to study liquation cracking in alloy 718, Metallurgical Transactions A, 1991; 22 (4), pp. 887-902.
[4] Hemsworth, B., Boniszewski, T. & Eaton N.F.: Classification and Definition of High Temperature Welding Cracks in Alloys, Metal Construction and British Welding Journal, 1969; 1 (1) pp. 5-16.
[5] Cross, C.E.: On the Origin of Weld Solidification Cracking, in Böllinghaus, T., and Herold, H. (Eds.): Hot Cracking Phenomena in Welds (Springer Berlin Heidelberg, 2005), pp. 3-18.
[6] Pellini, W.S.: Strain theory of hot tearing, n.a., 1952; 80, pp. 99-125.
[7] Prokhorov, N.N.: The technological strength of metals while crystallizing during welding, Welding Production, 1962; 9 (4), pp. 1-8.
[8] Prokhorov, N.N.: The problem of the strength of metals while solidifying during welding, Svarochnoe Proizvodstvo, 1956; 6, pp. 5-11.
[9] Senda, T., Matsuda, F., and Takano, G.: Studies on Solidification Crack Susceptibility for Weld Metals with Trans-Varestraint Test (2) Investigation for Commercially Used Aluminum and Aluminum Alloys, JOURNAL OF THE JAPAN WELDING SOCIETY, 1973; 42 (1), pp. 48-56.
[10] Matsuda, F., Nakata, K., Okada, H.: The VDR Cracking Test for

Solidification Crack Susceptibility on Weld Metals and Its Application to Aluminum Alloys (Materials, Metallurgy, Weldability), Transactions of JWRI, 1979; 8, pp. 85-95.
[11] Matsuda, F., Nakagawa, H., Nakata, K., Kohmoto, H., and Honda, Y.: Quantitative Evaluation of Solidification Brittleness of Weld Metal during Solidification by Means of In-Situ Observation and Measurement (Report I) : Development of the MISO Technique (Materials, Metallurgy & Weldability), Trans. JWRI, 1983; 12, pp. 65-72.
[12] Matsuda, F., Kohomoto, H., Yoshioki, H., Matsubara, Y.: Quantitative Evaluation of Solidification Brittleness of Weld Metal during Solidification by In-Situ Observation and Measurement (Report II) : Solidification Ductility Curves for Steels with the MISO Technique (Materials, Metallurgy & Weldability), Transactions of JWRI, 1983; 12, pp. 73-80.
[13] Bakir, N.: Numerical simulation of solidification crack formation during laser beam welding of austenitic stainless steels under external load, Welding in the world, 2015; 60 (5), pp. 1001-1008.
[14] Bakir, N., Gumenyuk, A., and Rethmeier, M.: Investigation of solidification cracking susceptibility during laser beam welding using an in-situ observation technique, Science and Technology of Welding and Joining 2018; 23 (3), pp. 234-240.
[15] Bakir, N., Pavlov, V., Zavjalov, S., Volvenko, S., Gumenyuk, A., and Rethmeier, M.: Development of a novel optical measurement technique to investigate the hot cracking susceptibility during laser beam welding, Welding in the World, 2019; 63 (2), pp. 435-441.
[16] DIN EN 10088-3:2014 Stainless steels – Part 3: Technical delivery conditions for semi-finished products, bars, rods, wire, sections and bright products of corrosion resisting steels for general purposes; German version EN 10088-3:2014, 2014.